Relativistic Impulse-Approximation Calculation of $\bar{p}$-Nucleus Elastic Scattering

B. C. Clark and S. Hama
The Ohio State University, Columbus, Ohio 43210

and

J. A. McNeil
Drexel University, Philadelphia, Pennsylvania 19104

and

R. L. Mercer
IBM Watson Research Laboratories, Yorktown Heights, New York 10598

and

L. Ray
University of Texas at Austin, Austin, Texas 78712

and

B. D. Serot
Department of Physics and Nuclear Theory Center, Indiana University, Bloomington, Indiana 47405

and

D. A. Sparrow and K. Stricker-Bauer
University of Pennsylvania, Philadelphia, Pennsylvania 19104
(Received 20 August 1984)

The first calculations of $\bar{p}$-nucleus elastic scattering using the relativistic impulse approximation are presented and compared with the recent 46.8-MeV $\bar{p}$-^{12}C elastic scattering data. The calculated cross sections agree well with the data. The differences between relativistic and nonrelativistic impulse-approximation calculations using the same input are small.

PACS numbers: 25.90.+k, 24.10.−i

The success of the relativistic impulse approximation (RIA)[1] in describing proton-nucleus elastic scattering cross sections and spin observables at intermediate energies is now well documented.[2,3] If this success is indeed a reflection of the importance of a relativistic treatment of the dynamics in the nucleon-nucleus system and not fortuitous, a relativistic treatment of antinucleon-nucleus scattering should also be successful. Recently $\bar{p}$-^{12}C elastic data at 46.8 MeV have been presented[4] which we use to test and compare the relativistic and nonrelativistic (NR) approaches.

In the absence of a calculable theory of hadronic interactions the impulse approximation plays the critical role of relating the empirical two-body scattering information to the $(A+1)$-body scattering system. The basis for the validity of the impulse approximation rests upon the fact that for sufficiently high energies the projectile-target particle scattering can be characterized in terms of the free two-body scattering. Medium corrections such as Fermi motion, Pauli blocking, and binding are small. In its simplest form the projectile-nucleus interaction consists of the projectile–target-nucleon T matrix folded with the nuclear density.

In the RIA the on-shell two-body scattering amplitude is written in terms of five independent amplitudes with scalar, pseudoscalar, vector, axial vector, and tensor Lorentz transformation properties,[1,2]

$$\hat{F} = F_S I_1 I_2 + F_P \gamma_1^5 \gamma_2^5 + F_V \gamma_1^\mu \gamma_{2\mu} + F_A \gamma_1^5 \gamma_1^\mu \gamma_2^5 \gamma_{2\mu} + F_T \sigma_1^{\mu\nu} \sigma_{2\mu\nu}, \quad (1)$$

where I, γ^5, γ^μ, and $\sigma^{\mu\nu}$ are Dirac matrices and the subscripts 1 and 2 are particle labels. The relativistic po-

tentials are generated by forming ground-state expectation values of $\hat{F}$ given by

$$U = -\frac{4\pi ik}{m}\sum_{i=1}^{A}\langle\Psi_0|\hat{F}_i|\Psi_0\rangle, \tag{2}$$

where k is the laboratory momentum of the $\bar{p}$ and Ψ_0 is the relativistic nuclear wave function. For a spin-zero nucleus with filled l,j subshells only scalar, S, vector, V, and tensor, T, potential terms survive. Each term of the potential is obtained by folding the amplitudes F_α ($\alpha = S,V,T$) with the corresponding densities ρ_α, where

$$\rho_S = \sum_{\text{occ}}\frac{2j+1}{4\pi}(|\phi_U|^2 - |\phi_L|^2), \quad \rho_V = \sum_{\text{occ}}\frac{2j+1}{4\pi}(|\phi_U|^2 + |\phi_L|^2), \quad \rho_T = 2\sum_{\text{occ}}\frac{2j+1}{4\pi}\phi_U\phi_L. \tag{3}$$

In Eq. (3), ϕ_U (ϕ_L) are the upper (lower) components of the relativistic single-particle wave function. These potentials enter into the Dirac equation according to their Lorentz character,

$$\{\vec{\alpha}\cdot\vec{p} + \beta[m + S(r)] + [V(r) + U_{\text{Coul}}(r)] - 2i\beta\vec{\alpha}\cdot\hat{r}T(r)\}\psi(\vec{r}) = E\psi(\vec{r}). \tag{4}$$

The Dirac representation of the two-body scattering amplitude is defined in the positive-energy domain to be equivalent to the usual Pauli form for on-shell scattering amplitudes. The important difference between the relativistic and NR treatments is the equation solved for the projectile; specifically the inclusion of virtual negative-energy scattering states. Tensor and vector-scalar density difference effects are minor by comparison.

There is some question about the applicability of the impulse approximation for projectile energies as low as 50 MeV. However, since the imaginary potentials have considerably larger radii than the ^{12}C nucleus the scattering is dominated by the nuclear tail region where medium corrections should be small. Furthermore, there are no corrections in $\bar{p}$ scattering arising from the identity of projectile and target particles. More formal support for the validity of the impulse approximation comes from the work of Gibbs and co-workers.[5]

The impulse approximation requires a complete set of two-body amplitudes as input. Because $\bar{N}N$ data is scarce, it is useful to exploit the connection between nucleons and antinucleons given by charge conjugation. Although any $\bar{N}N$ scattering diagram can be related to an NN diagram, the physical kinematical regions are different in general. Knowledge of one physical amplitude does not necessarily give information about the other. The one-meson-exchange diagrams are an important exception. In this case $\bar{N}N$ and NN amplitudes can be related by the G-parity operator. Under G parity a nucleon coupled to a meson becomes an antinucleon coupled to the same meson with a phase which is the G parity of the meson. Since the meson-exchange structure of the NN potential is reasonably well known, the equivalent $\bar{N}N$ potential can be constructed from it by G parity. To this must be added a complex potential to describe the annihilation process. This procedure has been carried out by several groups,[6,7] using a phenomenological annihilation potential with parameters adjusted so that the T matrix generated by the $\bar{N}N$ potential fits with the available data. We use the T matrix elements generated recently by Côté *et al.*[7] It should be emphasized that our analysis can be applied just as easily with the empirical $\bar{N}N$ amplitudes as soon as those are determined to sufficient accuracy.

The G-parity argument at the level of the Dirac equation for scattering from a nucleus cannot be made. Consider the N-nucleus Dirac equation (4) and ignore the small tensor contribution. The $\bar{p}$ wave function is the charge conjugate wave function ψ_c to proton wave function ψ, and is given by $\psi_c = i\gamma^2\psi^*$. If S and V are treated as numbers, it can be shown that ψ_c satisfies the same Dirac equation as ψ but with $\bar{p}$ scalar and vector potentials given by $S_{\bar{p}} = S_p^*$, $V_{\bar{p}} = -V_p^*$. This ignores the origin of S and V, which are bound-state nuclear matrix elements [see Eqs. (2) and (3)]. Proper treatment of the charge-conjugation properties of S and V in the Dirac equation would produce $\bar{p}$-antinucleus potentials, not very useful quantities at present.

We return now to the construction of the potentials in the impulse approximation. The optimization of Gurvitz, Dedonder, and Amado[8] has been used to relate the two-body amplitudes to the T matrix elements required in the projectile-nucleus system. This method eliminates certain first-order corrections to the impulse approximation and has the additional advantage that the T matrix elements are defined over the entire range of the projectile-target momentum transfer, not just the two-body

physical region of momentum q. This is important for this case because the nuclear densities in momentum space do not fall off fast enough to make the large-q behavior of F unimportant.

To complete the input to the optical potential the appropriate relativistic nuclear densities are required. In this work two models have been used. The first is based on relativistic mean-field theory (RMFT) calculations of Horowitz and Serot.[9] The second is a sum of Gaussians (SOG) form with the parameters fitted to electron scattering data.[10] For this case the tensor density is zero and the proton and neutron scalar and vector densities are all taken to be the same. The latter model was used for the comparison of relativistic and NR calculations.

The $\bar{p}$-nucleus scalar and vector potentials generated by folding F_α with the RMFT densities are shown in Fig. 1 along with the nonfolded potentials $F_\alpha(q=0)\rho_\alpha(r)$ for comparison. The real parts of S and V are both large and of opposite sign so that the effective NR real central potential[11] (shown along with the spin-orbit potential in Fig. 1) is small. The imaginary parts of S and V combine to produce a large imaginary effective potential. It is clear that F_α has a substantial range; the folded potentials have less central strength and larger range than the unfolded potentials. This is especially extreme for the imaginary potentials. In ^{12}C the rms radii for Im(S) and Im(V) are 4.10 and 3.61 fm, respectively, compared with an rms charge radius of 2.46 fm. The large extent of the absorptive potential will eliminate any possibility of orbiting phenomena as recently discussed by Kahana and Sainio.[12]

The cross sections calculated with these potentials are shown by solid and dashed lines in Fig. 2. The agreement between the full RIA calculation (solid line) and the data is excellent at all angles. The calculation with nonfolded potentials (dashed lines) poorly describes the Coulomb-nuclear interference region and the position of the minimum. Hence the phase of the amplitude and the size of the interaction region are sensitive to these ranges. Our calculations also agree well with the measured $\bar{p}$-^{12}C total reaction cross sections.[13]

The spin observables A_y and Q are shown in the lower portion of Fig. 2. Note that the calculations neglecting the force ranges are relatively structureless. Structure in the spin observables generally depends upon shape differences between the spin-orbit potential and the derivative of the central potential. In proton scattering at medium energies these differences arise largely from the nonlinear terms in the effective NR potential. For this case these terms are relatively smaller and the effects of the ranges much larger.

Because the nonlinear terms in antiproton scattering are smaller than in proton scattering one expects smaller differences between RIA and NR predictions. This is confirmed by the dash-dotted curves in Fig. 2 which display NR folding calculations using the SOG charge densities for protons and neutrons and $\bar{p}$-nucleon amplitudes in the Pauli

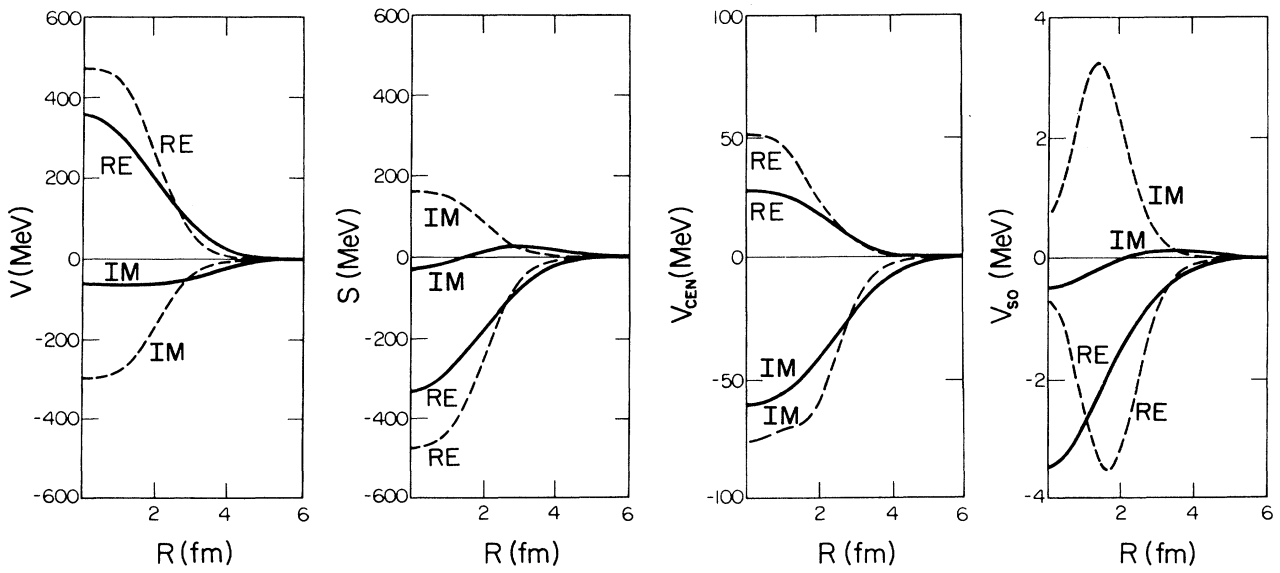

FIG. 1. RIA scalar and vector potentials and effective NR central and spin-orbit potentials using the RMFT densities (Ref. 9). For the solid curves the range of the two-body interaction is included whereas it is omitted in the dashed curves.

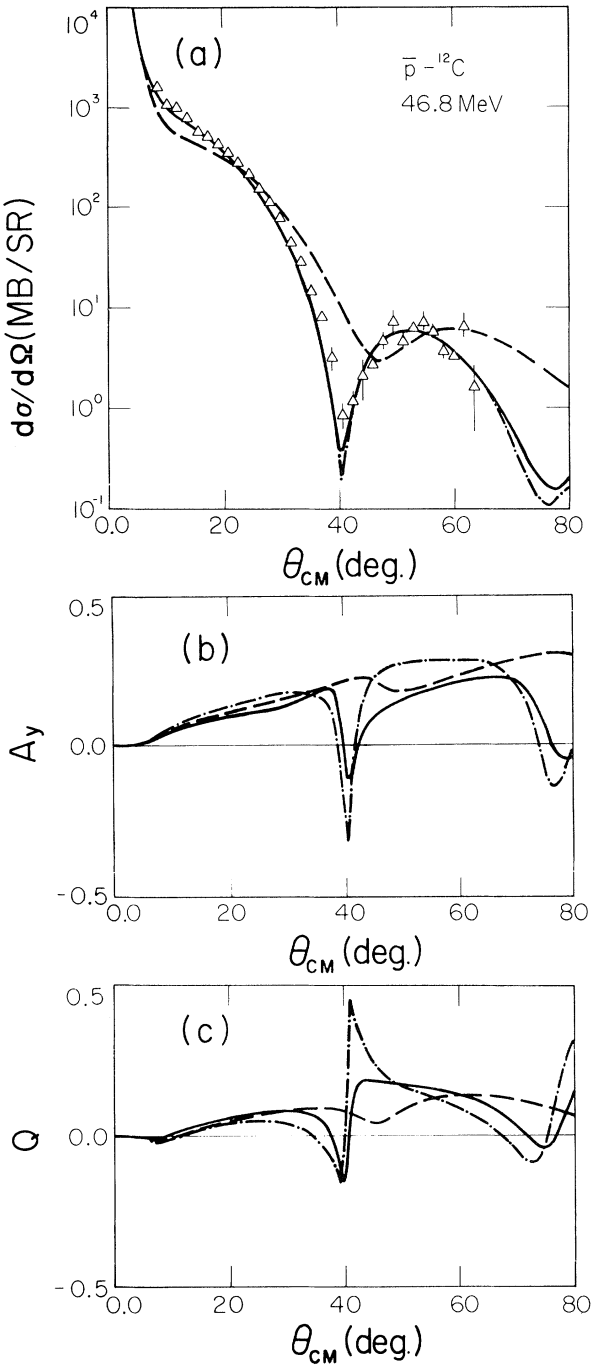

FIG. 2. Differential cross section, analyzing power (A_y), and spin rotation (Q) RIA predictions using the RMFT densities with the two-body range included (solid curves) and omitted (dashed lines) in comparison with data. NR predictions are indicated by the dash-dotted curves. RIA predictions using the SOG densities (see text) are indistinguishable from the solid curves.

form. In general a diminution of relativistic effects is associated with strong absorption and weak spin-orbit coupling as in the present case.

In conclusion, the RIA calculations for antiproton-nucleus scattering are in excellent agreement with the recent 46.8-MeV ^{12}C data. With respect to forward-angle cross sections the impulse approximation is valid, even at this low energy. The $\bar{p}$-N T matrix has a long range in coordinate space which must be included for even quantitative agreement with the data and which is responsible for the structure in the predicted spin observables. Differences between the RIA and NR models are small. This work is being extended to higher energies and other nuclei.

This research was supported in part by the National Science Foundation and the Department of Energy. One of the authors (B.D.S.) is a recipient of an Alfred P. Sloan Research Foundation Fellowship. We thank C. B. Dover, M. Lacombe, R. Vinh Mau, and M. E. Sainio for providing the $\bar{N}N$ amplitudes.

[1]J. A. McNeil, J. Shepard, and S. J. Wallace, Phys. Rev. Lett. **50**, 1439 (1983).

[2]J. Shepard, J. A. McNeil, and S. J. Wallace, Phys. Rev. Lett. **50**, 1443 (1983); B. C. Clark, S. Hama, R. L. Mercer, L. Ray, and B. D. Serot, Phys. Rev. Lett. **50**, 1644 (1983).

[3]R. D. Amado, J. Piekarewicz, D. A. Sparrow, and J. A. McNeil, Phys. Rev. C **28**, 2180 (1983).

[4]D. Garreta *et al.*, Phys. Lett. **135B**, 266 (1984).

[5]W. R. Gibbs, private communication. Work by W. R. Gibbs, W. B. Kaufmann, and D. Strottman was reported in Proceedings of the Conference on the Intersections Between Particle and Nuclear Physics, 23–30 May 1984, Steamboat Springs, Colorado (to be published).

[6]R. A. Bryan and R. J. N. Phillips, Nucl. Phys. **B5**, 201 (1968); C. B. Dover and J. M. Richard, Phys. Rev. C **21**, 1466 (1980); C. B. Dover, M. E. Sainos, and G. E. Walker, Phys. Rev. C **28**, 2368 (1983).

[7]J. Côté *et al.*, Phys. Rev. Lett. **48**, 1319 (1982).

[8]S. A. Gurvitz, J.-P. Dedonder, and R. D. Amado, Phys. Rev. C **19**, 142 (1979). See also J. A. McNeil, L. Ray, and S. J. Wallace, Phys. Rev. C **27**, 2123 (1983).

[9]C. J. Horowitz and B. D. Serot, Nucl. Phys. **A368**, 503 (1981).

[10]I. Sick, Nucl. Phys. **A218**, 509 (1974).

[11]B. C. Clark, S. Hama, and R. L. Mercer, in *Interactions Between Medium Energy Nucleons in Nuclei–1982,* edited by H. O. Meyer, AIP Conference Proceedings No. 97 (American Institute of Physics, New York, 1983), p. 260. Elimination of the lower components of the wave function in the Dirac equation yields, after a transformation, a second-order, Schrödinger equation in which the effective central and spin-orbit potentials are identifiable.

[12]S. W. Kahana and M. E. Sainio, Phys. Lett. **139B**, 231 (1984).

[13]K. Nakamura *et al.*, Phys. Rev. Lett. **52**, 731 (1984).